

Statistical properties of H α jets in the polar coronal hole and their implications in coronal activities

Youqian Qi¹, Zhenghua Huang¹, Lidong Xia¹, Hui Fu¹, Mingzhe Guo¹, Zhenyong Hou^{1,2}, Weixin Liu¹, Mingzhe Sun¹, and Dayang Liu¹

¹ Shandong Provincial Key Laboratory of Optical Astronomy and Solar-Terrestrial Environment, Institute of Space Sciences, Shandong University, Weihai, 264209 Shandong, China
e-mail: xld@sdu.edu.cn

² Now at School of Earth and Space Sciences, Peking University, Beijing 100871, China

December 15, 2021

ABSTRACT

Context. Dynamic features, such as chromospheric jets, transition region network jets, coronal plumes and coronal jets, are abundant in the network regions of the solar polar coronal holes.

Aims. We investigate the relationship between chromospheric jets and coronal activities (e.g., coronal plumes and jets).

Methods. We analyze observations of a polar coronal hole including the filtergrams that were taken by the New Vacuum Solar Telescope (NVST) at the H α -0.6 Å to study the H α jets, and the Atmospheric Imaging Assembly (AIA) 171 Å images to follow the evolution of coronal activities.

Results. H α jets are persistent in the network regions, only some regions (denoted as R1–R5) are rooted with discernible coronal plumes. With an automated method, we identify and track 1 320 H α jets in the network regions. We find that the average lifetime, height and ascending speed of the H α jets are 75.38 s, 2.67 Mm, 65.60 km s⁻¹, respectively. The H α jets rooted in R1–R5 are higher and faster than those in the others. We also find that propagating disturbances (PDs) in coronal plumes have a close connection with the H α jets. The speeds of 28 out of 29 H α jets associated with PDs are ≥ 50 km s⁻¹. In a case of coronal jet, we find that the speeds of both the coronal jet and the H α jet are over 150 km s⁻¹, suggesting that both cool and hot jets can be coupled together.

Conclusions. Based on our analyses, it is evident that more dynamic H α jets could release the energies to the corona, which might be the results of the development of Kelvin-Helmholtz instability (KHi) or small-scaled magnetic activities. We suggest that chromospheric jets, transition region network jets and ray-like features in the corona are coherent phenomena, and they are important tunnels for cycling energy and mass in the solar atmosphere.

Key words. Sun: chromosphere– Sun:corona– Sun: spicules– Sun:coronal jet– Sun: Coronal Plumes

1. Introduction

The chromosphere is dynamic and highly-structured, which links the photosphere and the corona. In the photosphere, the magnetic flux tubes build the magnetic network, which expands upward and appears as bright patches in the chromosphere, namely, chromospheric network. Therefore, the network boundaries in the chromosphere spatially coincide with the magnetic network concentrations in the photosphere. The chromospheric network boundaries are abundant with jet-like, fine-scale features, which are referred as spicules at the limb, mottles in the quiet sun and fibrils in active regions (e.g., Beckers 1968; Rouppe van der Voort et al. 2007; De Pontieu et al. 2007a, etc.). Spicules have been studied for more than a century and are still one of the most popular topics at the present days (see e.g., Beckers 1968; Sterling 2000; Tsiropoula et al. 2012, for extensive overviews)

Thanks to high spatio-temporal resolution observations, De Pontieu et al. (2007c) pointed out that there are two different types of spicules (Type-I & Type-II). The typical characteristic of Type-I spicules (also known as traditional spicules) is that they move up and down with the ascending speeds in the range of 15 – 40 km s⁻¹. The Type-I spicules have lifetimes of 150 – 400 s and heights of 4 – 8 Mm, and they are believed to result from magnetoacoustic shocks. In contrast, Type-II spicules rise with much higher speeds of ~ 100 km s⁻¹ and disappear rapidly with shorter lifetimes of 50 – 150 s. Type II spicules are suggested to be driven by magnetic reconnections. De Pontieu et al. (2007d) found that the Type-II spicules also undergo sideways swaying motion which is signature of Alfvén waves permeating with enough energy to heat the corona and accelerate the solar wind. With high-quality observations, the Type-II spicules have been found to combine three different types of motions: field-aligned flows, swaying motions and torsional motions, of which swaying and torsional motions are considered as a sign that spicules propagate along their axis with Alfvén waves at high speeds ranging from 100 – 300 km s⁻¹. With multi-wavelength observations, Type-II spicules often appeared to heat to the transition region temperatures, even up to the coronal temperatures (e.g., De Pontieu et al. 2011, 2014; Rouppe van der Voort et al. 2015). In the advanced 2.5D radiative MHD simulations, Martínez-Sykora et al. (2017) reproduced many observed properties of type II spicules with ~ 100 km s⁻¹ speeds and ~ 10 Mm heights, and also revealed that spicules could heat plasma to the corona by

dissipation of current which is due to ambipolar diffusion. The further numerical study showed that the dissipation through ambipolar diffusion of electrical currents could also explain why the observed spicules could reach a speed exceeding 100 km s^{-1} and heat to coronal temperatures (De Pontieu et al. 2017).

In active region plage regions, Hansteen et al. (2006) and De Pontieu et al. (2007a) analyzed $H\alpha$ observations and found that fibrils appear as short, dynamic and spicule-like features which have lifetimes of 3 – 6 minutes and show quasi-periodicity. These dynamic fibrils undergo ascent and descent motions with velocities of $10 - 35 \text{ km s}^{-1}$ at the initial phase, which are similar to that of Type-I spicules. Moreover, the numerical simulations demonstrated that these fibril-like features also show wave-behaviors. That could be formed when flows and oscillations leak from magnetic flux concentrations into chromosphere (*e.g.*, Hansteen et al. 2006; De Pontieu et al. 2007a; Heggland et al. 2007, 2011).

In quiet-Sun regions, mottles show as dark and spicule-like features against the disk in the wings of $H\alpha$. Similar to fibrils, the motions of some mottles also follow a parabolic path and they can be driven by shock waves (*e.g.*, Rouppe van der Voort et al. 2007; De Pontieu et al. 2007b).

With the spectroscopic data, Langangen et al. (2008) firstly used $\text{Ca II } 854.2 \text{ nm}$ line to investigate the rapid blueshifted excursions (RBEs) on disk, which are a sudden widening of line profile in the blue wing without an associated redshift. Combined with SJ images of $H\alpha$, these RBEs show as narrow streaks emanating from network (Rouppe van der Voort et al. 2009). The RBEs show velocities of $15 - 20 \text{ km s}^{-1}$ and a mean lifetime of 45 s. There are $\sim 10^5$ RBEs on the surface of disk at any moment. Recently, Sekse et al. (2012, 2013) found that RBEs also undergo three kinds of motions like spicules. Owing to the similarity, RBEs are interpreted as the on-disk counterparts of Type-II spicules and suggested to result from magnetic reconnection (Rouppe van der Voort et al. 2009).

Jet-like features are not only seen in the chromosphere, but also in the transition region and corona. In the transition region, network jets are small-scale structures, having lifetimes of 20 – 80 s and speeds of $80 - 250 \text{ km s}^{-1}$. A number of them appear as “inverse-Y” shape, which should be driven by magnetic reconnection (Tian et al. 2014). In the corona, coronal jets appear as transient collimated beams. More findings suggest that coronal jets are driven by magnetic reconnection and may be the source of mass and energy input to the upper solar atmosphere and the solar wind (see Raouafi et al. 2016, and the references therein). Plumes belong to another type of collimated structures, which are relatively large and stable. (see Wilhelm et al. 2011, and the references therein) and might supply plasma and energy for solar wind (*e.g.*, Tian et al. 2010, 2011; Fu et al. 2014; Liu et al. 2015; Huang et al. 2021).

There are PDs in coronal plumes with 10% - 20% intensity variations, periods of 10 - 30 minutes and speeds of $75 - 170 \text{ km s}^{-1}$ (*e.g.*, DeForest & Gurman 1998; Krishna Prasad et al. 2011). Furthermore, Tian et al. (2011) discovered that high-speed quasi-periodic outflows could be found in both plumes and inter-plume regions, and their speeds are similar to that of PDs. These outflows were suggested to be responsible for the generation of PDs (McIntosh et al. 2010). By following the evolution of spicules, Jiao et al. (2015) and Pant et al. (2015) concluded that the spicules can trigger PDs.

In the base of coronal plumes, Raouafi et al. (2008) found that coronal jets could contribute to rise and change brightness in the pre-existed plumes. Given that those coronal jets are rooted in the chromospheric network and are mainly triggered by magnetic reconnection, coronal plumes could also be powered by magnetic reconnection (for an extensive overview, see Raouafi et al. 2016). Furthermore, Raouafi & Stenborg (2014) and Panesar et al. (2018) found that a great number of jets and transient bright points frequently occurred in the bases of coronal plumes and these features could be the main energy source for coronal plumes. In fact, the scenario that coronal plumes are driven by the magnetic reconnection between the unipolarity magnetic features and nearby small-scale bipolar has been proposed much earlier (*e.g.*, Wang & Sheeley 1995; Wang et al. 1997; Wang & Muglach 2008).

Since there are many kinds of jet-like features rooted in network regions, it is natural to ask whether there is any connection among them or not. Aiming at this question, Qi et al. (2019, hereafter Paper I) developed an automatic method to identify and track network jets. They statistically analyzed a set of transition region network jets in the same network region, and they found that network jets in the root of coronal plumes have lifetime, height and speed averaging at 45.6 s, $8.1''$ and 131 km s^{-1} , significantly more dynamic than those in the region without discernible plume, which have longer lifetime of 50.2 s, smaller height of $5.5''$ and lower speed of 89 km s^{-1} in average. Paper I suggested that only more energetic network jets (likely with speeds more than 100 km s^{-1}) can feed plasma to the corona. In the present study, we further investigate the possible relationship between chromospheric jet-like features (*e.g.*, spicules, fibrils, mottles or RBEs) and coronal activities. To achieve this, we analyzed data obtained with the ground-based 1-m NVST (Liu et al. 2014; Xiang et al. 2016) installed at the Fuxian Lake Solar Observing Stations operated by Yunnan Astronomical Observatories in China and the space-borne AIA (Lemen et al. 2012) and the Helioseismic and Magnetic Imager (HMI, Schou et al. 2012) aboard the Solar Dynamics Observatory (SDO, Pesnell et al. 2012).

The paper is organized as follows. The observations and methodology are described in Sect. 2. The results are shown in Sect. 3. The discussion and conclusions are given in Sect. 4 and in Sect. 5, respectively.

2. Observations

The data set analyzed in this study was taken on 2018 September 15 targeting on a polar coronal hole. The observations include filtergrams taken by NVST at the $H\alpha - 0.6 \text{ \AA}$ with a bandpass of 0.25 \AA , EUV images taken at 171 \AA and 193 \AA passbands by AIA and line-of-sight magnetograms by HMI.

The NVST data were taken from 09:29 UT to 10:03 UT including a series of $H\alpha$ images with a cadence of 6 s and a spatial scale of $0.136 \text{ arcsec/pixel}$. The field-of-view covers a $144'' \times 144''$ region. The stabilization of the $H\alpha$ image series is performed with a fast sub-pixel image registration algorithm by the instrument team (Yang et al. 2015).

The AIA and HMI data were downloaded from JSOC. The cadences of the AIA 171 \AA data and HMI line-of-sight magnetograms are 12 s and 45 s, respectively. The spatial resolutions of the AIA and HMI data are $1.2''$. The AIA and HMI data are prepared with standard procedures provided by the instrument teams, and the level 1.5 data are analyzed.

The $H\alpha$ images have been transposed and rotated clockwise by 90 degrees to fit into the Helioprojective-Cartesian coordinate system as used in AIA and HMI data. Bad images in $H\alpha$ data have been manually removed and replaced by artificial ones obtained from interpolation of nearby good frames. The network lanes that present as magnetic concentrations on HMI magnetograms and clusters of bright dots on $H\alpha$ images are used to align the corresponding images. We make use of AIA 1600 Å as reference to align the $H\alpha$ images and 171 Å images. And we manually check the alignment between 1600 Å and 171 Å using referent features, despite images from different passbands of AIA have been aligned with each other by the data processing pipeline.

In Fig. 1, we show the studied regions seen with AIA, HMI and $H\alpha -0.6$ Å around 09:28 UT. The region is part of the polar coronal hole (see Fig. 1(a)). In Fig. 1(b), even though the region is part of the polar region, we can see typical magnetic structures of network regions (e.g., Xia et al. 2003, 2004). The network regions also could be clearly seen in NVST $H\alpha -0.6$ Å images (see the bright lanes in Fig. 1(d)). We could clearly see lots of jet-like features rooting in the network lanes in the $H\alpha -0.6$ Å images. Given that this region is close to the north polar, these jets exhibit upward motions from the $H\alpha$ off-bands filter, so we defined these jet-like features as the $H\alpha$ jets in this paper. In the coronal images (AIA 171 Å), we also see plume-like and/or jet-like features rooted in coronal bright points at some locations in the coronal hole (Figs. 1(a)&(e)). Figure 1(c) shows PDs with a simple bandpass filter method on the AIA 171 Å images.

3. Data Analyses and Results

In $H\alpha$ images, jets appear as dark features. In Fig. 1 and the associated animation, we can see that $H\alpha$ jets are abundant in the network regions. To identify these jets, we upgrade the automatic algorithm that was described in Paper I and some key definitions are given in Huang et al. (2017). Note that “local peaks” as defined in Huang et al. (2017) are replaced by “local trough”, or in other words, multiply the $H\alpha$ intensity by -1 to identify “local peaks”. In practical operations, we trace them from their bases to tops to obtain their full trajectories and then deduce their lifetimes and speeds.

3.1. Statistics of $H\alpha$ jets

By applying the automatic algorithm on the full field-of-view, we identify and trace 1320 $H\alpha$ jets during the observing period of time. We proceed a statistics on their lifetimes, heights and speeds. Figure 2 shows the distributions of these properties. We obtain an average lifetime of 75.38 ± 33.08 s, an average height of 2.67 ± 1.03 Mm and an average ascending velocity of 65.60 ± 42.59 km s^{-1} . In the speed regime, 44% of $H\alpha$ jets fall in the range between 10 km s^{-1} and 50 km s^{-1} . These are consistent with those found by Pasachoff et al. (2009), and this group of $H\alpha$ jets is likely triggered by shocks (Hollweg 1982) and/or leakage of p-modes (De Pontieu et al. 2004). About 40% of $H\alpha$ jets are in the range of 50–100 km s^{-1} , which are in accord with Type-II spicules. About 16% of $H\alpha$ jets have speeds higher than 100 km s^{-1} , in which those having speeds more than 150 km s^{-1} account for about 5%. Such high velocities agree well with those reported for Type-II spicules off the limb (e.g., De Pontieu et al. 2011, 2017; Martínez-Sykora et al. 2017). In observations, we also find plenty of $H\alpha$ jets moving up to the highest point, then disappear. We also find that quite a few $H\alpha$ jets undergo obvious swaying motions, but it is not easy to measure their periods because the lifetime of jets is too short to follow a complete cycle. Lacking of the spectroscopic observations, the torsional motions could be not identified.

From Fig. 1(d), there are numerous $H\alpha$ jets in the network regions. We select two full and clear network regions (see green-dashed lines) in Fig. 1(d) and count the number of $H\alpha$ jets as shown in Fig. 3. The number of $H\alpha$ jets is ~ 58 per network region at any given time, which is consistent with reported spicules in previous studies (e.g., Lynch et al. 1973; Moore et al. 2011). Based on the similarity in lifetime, speed, height, spatial extent, location near network, birthrate, we suggest that the above analyzed $H\alpha$ jets are extremely similar to spicules.

3.2. $H\alpha$ jets in the roots of coronal plumes

In Fig. 1, we see that plumes (plume-like features) are rooted in the regions of R1–R5, while they are hardly seen in other regions as determined from the AIA 171 Å images. We also see coronal bright points are clearly shown in R1–R5. In the $H\alpha$ images, we find 373 $H\alpha$ jets rooted in R1–R5 and 947 rooted in the rest regions. In Fig. 4, we compare the statistics of $H\alpha$ jets rooted in two kinds of regions. The normalized distributions of the lifetimes in $H\alpha$ jets in these two regions are almost identical. The significant differences are shown in the distributions of heights and speeds. Despite the distributions of each parameter from two kinds of regions are largely overlapped, the distributions of heights and speeds from regions rich in coronal plumes (R1–R5) bias toward higher and faster wings than those from the regions poor in coronal plumes. Specifically, $H\alpha$ jets in R1–R5 have height averaging at 3.01 ± 1.07 Mm, and speed averaging at 81.2 ± 48.3 km s^{-1} . In contrast, the average height and speed of the $H\alpha$ jets rooted in other regions poor in coronal plumes are 2.48 ± 0.95 Mm and 56.9 ± 36.3 km s^{-1} , respectively.

Our study in Paper I shows that transition region network jets in the footpoints of coronal plumes also tend to be more dynamic (higher and faster) than those in other regions. Together with the consistent results found here in $H\alpha$ jets, we might have two hypotheses: a cascade effect might exist in these phenomena that dynamic $H\alpha$ jets power network jets and then dynamic network jets power coronal plumes; alternatively, high speed $H\alpha$ jets, network jets and coronal plumes are three different counterparts of the same physical processes (e.g., compression of magnetic elements (Wang et al. 2016)). A phenomenon consisting of multi-thermal structures is quite common in many coronal dynamics with more rapid evolution, such as coronal jets (e.g., Sterling et al. 2015; Shen et al. 2017; Huang et al. 2018b, 2020), flaring events (e.g., Huang et al. 2014, 2018a; Wei et al. 2020) and coronal bright points (e.g., Madjarska et al. 2012; Huang 2018), apart from the relatively static events like coronal plumes.

3.3. $H\alpha$ jets and PDs in coronal plumes

In order to trace PDs, we apply the simple bandpass filter on the AIA 171 Å images. We filter out the signals with the period shorter than 10 minutes and longer than 30 minutes. The detailed method is described in Jiao et al. (2015), and the results are shown in Fig. 1(c). In the associated animation of Fig. 1, PDs in R1–R5 can be clearly seen. Since artificial periodicity near the cutoff periods might be introduced artificially (Auchère et al. 2016; Kayshap et al. 2020), we choose manually and analyze further those PDs also showing discernible signals in the original images. We further investigate in detail the connection between PDs and the $H\alpha$ jets in their footpoint regions, and an example is given in Fig. 5. From Figs. 5(A)&(B) and the associated animations, we find that the footpoints of $H\alpha$ jets and PDs root in the same region, and the directions of their extensions are consistent with each other. For this reason, we believe that some $H\alpha$ jets and PDs might share the same magnetic flux tubes. Figure 5(C) shows a time-distant diagram along the PDs (see yellow arrow in Fig. 5(A)). The blue-dashed lines mark the locations of PDs. Figure 5(D)&(E) display the maximum height and ascending speed of the $H\alpha$ jets along the same path as the PDs observed at different time. Combined the panels (C), (D) and (E), we find that there is always a $H\alpha$ jet appearing before presence of a PD and also having the same orientation as that of the PD (denoted by red arrows in panel (D) / (E)). We also notice that many $H\alpha$ jets are rooted in the footpoints of PDs but not all of them are followed by PDs. So there is an obvious question what kind of $H\alpha$ jets are associated with PDs. In Figs. 5(D)&(E), for the same series of PDs we can see that the $H\alpha$ jets appear to be higher and/or faster before the presence of PDs. For the series of PDs shown in Fig. 5, the $H\alpha$ jets appearing just before PDs have an average height of 3.5 Mm and an average ascending velocity of 91.2 km s^{-1} , in contrast to 3.0 Mm and 73.9 km s^{-1} for those appear at the other times. This seems like that the $H\alpha$ jets corresponding to the PDs are more dynamic than those not associated with PDs. To confirm this, we investigate all PDs identified in R1–R5, which include six series of them in total. In these PDs, we trace 29 associated $H\alpha$ jets and show the histograms of their lifetimes, heights and speeds in Fig. 6. Although the average height and speed of these $H\alpha$ jets do not have much difference from those rooted with coronal plumes, we can see that the almost all (except one) $H\alpha$ jets followed by PDs have speeds of about or more than 50 km s^{-1} . This implies that only those chromospheric jets with speeds $\geq 50 \text{ km s}^{-1}$ can proceed PDs. This conclusion, however, requires further observational, theoretical and/or numerical investigations. The average lifetime of these $H\alpha$ jets is significantly larger, but this is mainly due to the small samples as there are four having lifetimes larger than 200 s.

We further select a cluster of $H\alpha$ jets existed in the vicinity of PDs (see between two red-dashed lines of Fig. 5(B)) and analyze their dynamics when the PDs appear. We compare the average height and speed of the $H\alpha$ jets when PDs are shown and those when not shown. We find that heights and speeds of the groups of $H\alpha$ jets with PDs are greater than those of $H\alpha$ jets not associated with PDs. The $H\alpha$ jets associated with PDs have heights averaging at $3.47 \pm 0.06 \text{ Mm}$, and speeds averaging at $91.2 \pm 32.8 \text{ km s}^{-1}$. In contrast, the average height and speed of the $H\alpha$ jets not associated with PDs are $3.06 \pm 0.67 \text{ Mm}$ and $73.4 \pm 35.6 \text{ km s}^{-1}$, respectively. Since the cross-section of a PD is much wider than a single $H\alpha$ jet, it is difficult to associate a particular jet to the PD. Therefore, it remains possible that PDs are preceded by a set of $H\alpha$ jets, rather than a single one.

3.4. The relation between $H\alpha$ jets and a coronal jet

Wang (1998) suggested that macrospicules seen in $H\alpha$ jets and He II 304 jets are also direct manifestations of magnetic reconnection. Given that magnetic reconnection can trigger coronal jets, we investigate whether $H\alpha$ jets have any connection with a faint coronal jet or not. In Fig. 7 and the associated animation, we show the evolution of the coronal jet observed in AIA 171 Å and the $H\alpha$ jets rooted in the same region. From Fig. 7(A), we can see that a coronal jet exists on the side of the footpoint of a coronal loop. In the animation, we clearly see that the loop expands from the bright base and form a blowout coronal jet at 09:50:28 UT, which can reach a height of about 9 Mm. In Fig. 7(C), the blue-dashed lines mark the location of the coronal jet, the speed of the coronal jet is about 158 km s^{-1} . We also find that a $H\alpha$ jet blows up from the footpoints of the loops at 09:48:30 UT, just before initiation of the coronal jet (see Fig. 7(B)). The development of the $H\alpha$ jet is well consistent with that of the coronal jet, including their spatial extensions and directions. This $H\alpha$ jet has a height of about 2.3 Mm and a rising speed of about 180 km s^{-1} . The speed of the $H\alpha$ jet is similar with that of the coronal jet. Therefore, we suggest that the coronal jets might be seen as the extension of part of $H\alpha$ jets. Unfortunately, this coronal jet is the only case found in the present observations. Further study in statistics is required to confirm our conclusion.

4. Discussion

In Paper I, we studied the relation between transition region network jets and coronal plumes. In the present work, we focus on chromospheric jet-like features observed in $H\alpha - 0.6 \text{ Å}$, namely $H\alpha$ jets. In agreement with Paper I, we found that the network regions where the coronal counterparts are active with coronal bright points and plumes tend to produce $H\alpha$ jets with more dynamic characteristics (i.e., larger heights and faster speeds) than those from the other network regions. Given that $H\alpha$ jets, network jets and coronal plumes may be associated with magnetic reconnection, it is possible that the energy produced by magnetic activities could transfer from fine structures in the low solar atmosphere to those in the corona.

In this paper, we find a few examples that $H\alpha$ jets have a one-to-one correspondence with PDs in spatial and temporal. The $H\alpha$ jets associated with PDs are usually faster and higher than the others. What's more, Wang et al. (1998) found that He II 304 Å jets are always associated with $H\alpha$ jets, but not all the $H\alpha$ jets are associated with He II 304 Å jets. We find that the faster and higher $H\alpha$ jets have a certain relationship with coronal jets. Perhaps, only parts of $H\alpha$ jets which are more energetic can reach the low corona and also be seen in He II 304 Å.

Why the $H\alpha$ jets are higher and faster at the roots of coronal plumes and jets? We will discuss the following possible mechanisms.

The first interpretation is associated with the generation of transverse wave induced KHi in $H\alpha$ jets. It has been proved that chromospheric jets usually accompany transverse motions with amplitudes up to $10 - 25 \text{ km s}^{-1}$ (De Pontieu et al. 2007d), which are generally interpreted as kink waves (He et al. 2009). Such waves are possible to induce the KHi due to velocity shear between magnetic structures and background medium (e.g., Terradas et al. 2008; Antolin et al. 2018, etc.). Antolin et al. (2018) considered the KHi induced by kink motions and attributed some observational properties of spicules to the development of KHi eddies. The small spatial structures induced by the KHi can help the dissipation of wave energy, and thus playing an important role in an understanding temperature increase of magnetic structures (e.g., Guo et al. 2019; Karampelas et al. 2019). In addition, Lau & Liu (1980) pointed out that if a longitudinal flow exceeds a criterion, the magnetized plasma is unstable. With the IRIS observations, Li et al. (2018b) found that the KHi could develop due to the strong shear (more than 204 km s^{-1}) between two blowout jets. In the case of kink waves with longitudinal flows, the criterion for developing the KHi has been discussed in many literatures, (e.g., Andries & Goossens 2001; Zhelyazkov et al. 2016; Li et al. 2018b). The threshold was derived by Andries & Goossens (2001) from eigen-mode analysis in a cylindrical model. It reads $U = V_{Ai}(1 + B_e/B_i \sqrt{\rho_i/\rho_e})$, where U (V_{Ai}) represents the flow (Alfvén) speed inside a jet, $B_i(\rho_i)$ and $B_e(\rho_e)$ are the magnetic field strength (density) in a jet and the ambient region, respectively. In spicules, the density and magnetic field of a chromospheric jet is about $3 \times 10^{10} \text{ cm}^{-3}$ and 40 G, respectively. Assume those for the ambient regions are $1 \times 10^9 \text{ cm}^{-3}$ and 10 G (see Tsiropoula et al. 2012; Sterling 2000; Centeno et al. 2010, and references therein). Generally, the Alfvén speed in the chromosphere is 40 km s^{-1} (De Pontieu et al. 2007d), indicating that the KHi can be induced in spicules when the upflow speed exceeds 98 km s^{-1} . Furthermore, Zhelyazkov et al. (2016) studied the propagating of kink waves in EUV jets in vertical magnetic tubes. They found that kink waves could become unstable when flow velocity exceeds 112 km s^{-1} . In Fig. 4, we can see that 28.4% $H\alpha$ jets have higher speed (more than 110 km s^{-1}) in R1–R5, while only 8.3% $H\alpha$ jets with such high speed in other regions. This means that in aforementioned observations, the KHi is possible to develop in faster $H\alpha$ jets in R1–R5. Due to the development of the KHi, the faster $H\alpha$ jets are possible to dissipate energy into higher atmospheres. Moreover, Cavus & Kazkapan (2013) proposed that the KHi might be a mechanism for the formation of magnetic reconnection. This means that the $H\alpha$ jets with KHi might be able to heat the corona. However, more detailed simulations should be considered in future studies.

Another possible interpretation is the interaction strength among small-scaled magnetic elements in the network region. For R1–R5, there are dominant network fields and some small-scale opposite-polarity fields in Fig. 1(b). Wang et al. (2016) proposed that the convergence of the base flux could trigger coronal plumes. The interaction of magnetic flux concentrations with constantly weak fields could result in strong magnetic tension. The strong magnetic tension which is amplified and transported upward through ambipolar diffusion could produce numerical faster spicules (more than 100 km s^{-1}) in 2.5D simulation (Martínez-Sykora et al. 2017). In addition, same as the 2.5D numerical simulation, Ding et al. (2011) also showed that the stronger magnetic field could produce higher up-flows velocities. These simulations mean that there are a great possibility of rapid jets in network field with weak opposite magnetic elements, and these jets might have coronal connection. Using high-spatial-resolution and high-time-cadence observations of the Goode Solar Telescope (GST, Goode et al. 2010; Cao et al. 2010), Samanta et al. (2019) provided observations from the photosphere to the chromosphere and the corona and supported that these chromospheric jets ($\sim 50 \text{ km s}^{-1}$) are driven by the interaction between strong network fields with small-scale opposite-polarity fields, of which have a good coronal connection. By performed order-of-magnitude estimation of energies, the authors estimated that these spicules supply enough energy into the corona. These speeds of jets are smaller than that in our results because the FOV in Samanta et al. (2019) is close to the center of disk. With respect to the relation between the chromospheric jets and coronal activities, the mixed-polarity magnetic fields could result in shuffling and further braiding of small-scale magnetic field lines, which produce magnetic reconnection at braiding boundaries and power the corona. By the same, Li et al. (2018a) proposed that the dissipation of electric currents due to the effect of small-scale weak magnetic activities (included spicules) could effectively heat corona at low heights. In addition, Priest et al. (2002) showed that the formation and dissipation of current sheets along these separatrices resulting from highly fragmented photospheric magnetic configurations could be an important contribution to coronal heating. This means that the activities of mixed-polarity on small scales might have enough power to coronal activities. In Fig. 1(d), we see that $H\alpha$ jets locate near the dominant network fields, but the lower resolution of magnetic fields measurements affect the detection of weak magnetic elements at the footpoints of $H\alpha$ jets. Further studies using high spatial-temporal resolution observations of the photosphere (such as the Goode Solar Telescope (GST), the forthcoming Daniel K. Inouye Solar Telescope (DKIST) and the planned Chinese Advanced Solar Observatories–Ground-based (ASO-G)) should shed more light on this topic.

Our analyses here have shown that $H\alpha$ jets with coronal responses tend to be higher and faster. Whether there are critical height and speed for a $H\alpha$ jet having coronal response should be investigated both theoretically and observationally. As discussed above, it may have different answers based on different mentioned mechanisms. Based on the present observations, we cannot find evidence of KHi due to the spatial and temporal resolutions. HMI magnetograms show clearly that a number of small-scale magnetic elements appear and disappear in the footpoints of these $H\alpha$ jets (see the animation associated with Fig. 1). Although the observed region is pretty much closed to the limb, the observations still give a hint of a degree of magnetic dynamics. Therefore, with the present observations, we are more favorable with the scenario of that more powerful interaction between small-scale magnetic elements tends to generate more dynamic phenomena. However, the KHi scenario cannot be ruled out within the present circumstance. In the near future, we will study in-depth how much initial energy of chromospheric jets is required to have coronal responses based on the above-mentioned mechanism.

5. Conclusions

In this paper, we analyzed observations taken by the 1-m New Vacuum Solar Telescope at a passband $H\alpha - 0.6 \text{ \AA}$. Thanks to the higher spatial and temporal resolution of the data, we were able to trace the evolutions of $H\alpha$ jets over time. Using an upgraded automated detection algorithm, we carried out a statistical study of $H\alpha$ jets. Using the algorithm, we identified and traced 1 320 $H\alpha$ jets in the data set. We found that the average lifetime, height and ascending speed of the $H\alpha$ jets are 75.38 s, 2.67 Mm,

65.60 km s⁻¹, respectively. These characteristics of the events agree well with those of Type-II spicules. In addition, we found that the H α jets occur in network regions where magnetic concentrations are present. We believe that the H α jets are corresponding to spicules or the on-disk counterparts of spicules.

We found that H α jets rooted in the footpoint regions of coronal plumes have an average lifetime of 76.1 \pm 35.0 s, an average height of 3.01 \pm 1.07 Mm and an average ascending velocity of 81.2 \pm 48.3 km s⁻¹. While the H α jets in the rest regions are having an average lifetime of 75.0 \pm 32.0 s, an average height of 2.48 \pm 0.95 Mm and an average ascending velocity of 56.9 \pm 36.3 km s⁻¹, these results show that the H α jets associated with coronal plumes are on average higher and more dynamic than those not with coronal plumes. Can these jets possibly provide energy to sustain a coronal plume? In corona, radiation cooling time is expressed as $\tau_{rad}(n_0, T_0) = \frac{9}{5} \frac{k_B T^{5/3}}{n \Lambda_0}$ in the corona (Aschwanden & Terradas 2008), taking in typical parameters of corona and plumes, where the radiative loss rate $\Lambda_0 \sim 10^{-17.73} \text{ ergs/cm}^3$, temperature $T \sim 1.0 \text{ MK}$ and density $n \sim 10^9 \text{ cm}^{-3}$, then we found the radiation cooling time scale is in the order of 1000 s. While the H α jets in the footpoint of a plume studied here present repeatedly in a time scale of about 80 s, much less than the radiation cooling time in the corona, it suggests that H α jets may provide energy continuously to sustain coronal plumes.

To determine exactly what type of H α jets might link to coronal activities, we further investigated the connection between H α jets and the PDs in plumes. We found that there are always H α jets appearing before the initiation of PDs and extending in the same directions of the PDs. Almost all these jets (28 out of 29) have speeds $\geq 50 \text{ km s}^{-1}$, thus we suggest that only those H α jets exceeding a certain velocity can be precursors of PDs.

A fade coronal jet with a speed of about 160 km s⁻¹ was also observed. We found that this coronal jet was accompanied by a H α jet that has a speed comparable to that of the coronal jet, suggesting that the coronal jet might be the extension of the part of H α jets.

In agreement with Paper I, present studies confirmed that small-scaled jet-like features in the solar lower atmosphere can directly connect to coronal activities. Given that most H α jets observed here are likely spicules in the chromosphere, we suggest that H α jets, if dynamic to a certain degree, can sufficiently power the corona. Combined the results shown in Paper I, we suggest that spicule-like features in the chromosphere, transition region network jets and ray-like features in the corona are coherent phenomena, and they are important tunnels for cycling energy and mass in the solar atmosphere.

Acknowledgments: We are grateful to the anonymous reviewer for the constructive comments and suggestions. L.X. and Y.Q. are supported by National Natural Science Foundation of China (NSFC) under contract No. 41974201. Z.H. thanks financial supports from NSFC under contract No. U1831112 and the Young Scholar Program of Shandong University, Weihai (2017WHWLJH07). H.F. is supported by NSFC contract No. U1931105. W.L. is supported by NSFC contract No. U1931122. M.S. is supported by NSFC contract No. 41627806. We would like to thank the NVST operation team for their hospitality during the observing campaign and preparation of the data. The data used are also courtesy of NASA/SDO, the AIA and HMI teams and JSOC.

References

- Andries, J. & Goossens, M. 2001, A&A, 368, 1083
 Antolin, P., Schmit, D., Pereira, T. M. D., De Pontieu, B., & De Moortel, I. 2018, ApJ, 856, 44
 Aschwanden, M. J. & Terradas, J. 2008, ApJ, 686, L127
 Auchère, F., Froment, C., Bocchialini, K., Buchlin, E., & Solomon, J. 2016, ApJ, 825, 110
 Beckers, J. M. 1968, Sol. Phys., 3, 367
 Cao, W., Gorceix, N., Coulter, R., et al. 2010, Astronomische Nachrichten, 331, 636
 Cavus, H. & Kazkapan, D. 2013, New A, 25, 89
 Centeno, R., Trujillo Bueno, J., & Asensio Ramos, A. 2010, ApJ, 708, 1579
 De Pontieu, B., Erdélyi, R., & James, S. P. 2004, Nature, 430, 536
 De Pontieu, B., Hansteen, V. H., Rouppe van der Voort, L., van Noort, M., & Carlsson, M. 2007a, ApJ, 655, 624
 De Pontieu, B., Hansteen, V. H., Rouppe van der Voort, L., van Noort, M., & Carlsson, M. 2007b, in Astronomical Society of the Pacific Conference Series, Vol. 368, The Physics of Chromospheric Plasmas, ed. P. Heinzel, I. Dorotović, & R. J. Rutten, 65
 De Pontieu, B., Martínez-Sykora, J., & Chintzoglou, G. 2017, ApJ, 849, L7
 De Pontieu, B., McIntosh, S., Hansteen, V. H., et al. 2007c, PASJ, 59, S655
 De Pontieu, B., McIntosh, S. W., Carlsson, M., et al. 2011, Science, 331, 55
 De Pontieu, B., McIntosh, S. W., Carlsson, M., et al. 2007d, Science, 318, 1574
 De Pontieu, B., Title, A., & Carlsson, M. 2014, Science, 346, 315
 DeForest, C. E. & Gurman, J. B. 1998, ApJ, 501, L217
 Ding, J. Y., Madjarska, M. S., Doyle, J. G., et al. 2011, A&A, 535, A95
 Fu, H., Xia, L., Li, B., et al. 2014, ApJ, 794, 109
 Goode, P. R., Coulter, R., Gorceix, N., Yurchyshyn, V., & Cao, W. 2010, Astronomische Nachrichten, 331, 620
 Guo, M., Van Doorselaere, T., Karampelas, K., et al. 2019, ApJ, 870, 55
 Hansteen, V. H., De Pontieu, B., Rouppe van der Voort, L., van Noort, M., & Carlsson, M. 2006, ApJ, 647, L73
 He, J., Marsch, E., Tu, C., & Tian, H. 2009, ApJ, 705, L217
 Heggland, L., De Pontieu, B., & Hansteen, V. H. 2007, ApJ, 666, 1277
 Heggland, L., Hansteen, V. H., De Pontieu, B., & Carlsson, M. 2011, ApJ, 743, 142
 Hollweg, J. V. 1982, ApJ, 257, 345
 Huang, Z. 2018, ApJ, 869, 175
 Huang, Z., Madjarska, M. S., Koleva, K., et al. 2014, A&A, 566, A148
 Huang, Z., Madjarska, M. S., Scullion, E. M., et al. 2017, MNRAS, 464, 1753
 Huang, Z., Mou, C., Fu, H., et al. 2018a, ApJ, 853, L26
 Huang, Z., Xia, L., Nelson, C. J., et al. 2018b, ApJ, 854, 80
 Huang, Z., Zhang, Q., Xia, L., et al. 2021, Sol. Phys., 296, 22
 Huang, Z., Zhang, Q., Xia, L., et al. 2020, ApJ, 897, 113
 Jiao, F., Xia, L., Li, B., et al. 2015, ApJ, 809, L17
 Karampelas, K., Van Doorselaere, T., & Guo, M. 2019, A&A, 623, A53
 Kayshap, P., Srivastava, A. K., Tiwari, S. K., Jelínek, P., & Mathioudakis, M. 2020, A&A, 634, A63

- Krishna Prasad, S., Banerjee, D., & Gupta, G. R. 2011, *A&A*, 528, L4
 Langangen, Ø., De Pontieu, B., Carlsson, M., et al. 2008, *ApJ*, 679, L167
 Lau, Y. Y. & Liu, C. S. 1980, *Physics of Fluids*, 23, 939
 Lemen, J. R., Title, A. M., Akin, D. J., et al. 2012, *Sol. Phys.*, 275, 17
 Li, K. J., Xu, J. C., & Feng, W. 2018a, *ApJS*, 237, 7
 Li, X., Zhang, J., Yang, S., Hou, Y., & Erdélyi, R. 2018b, *Scientific Reports*, 8, 8136
 Liu, J., McIntosh, S. W., De Moortel, I., & Wang, Y. 2015, *ApJ*, 806, 273
 Liu, Z., Xu, J., Gu, B.-Z., et al. 2014, *Research in Astronomy and Astrophysics*, 14, 705
 Lynch, D. K., Beckers, J. M., & Dunn, R. B. 1973, *Sol. Phys.*, 30, 63
 Madjarska, M. S., Huang, Z., Doyle, J. G., & Subramanian, S. 2012, *A&A*, 545, A67
 Martínez-Sykora, J., De Pontieu, B., Hansteen, V. H., et al. 2017, *Science*, 356, 1269
 McIntosh, S. W., Innes, D. E., de Pontieu, B., & Leamon, R. J. 2010, *A&A*, 510, L2
 Moore, R. L., Sterling, A. C., Cirtain, J. W., & Falconer, D. A. 2011, *ApJ*, 731, L18
 Panesar, N. K., Sterling, A. C., Moore, R. L., et al. 2018, *ApJ*, 868, L27
 Pant, V., Dolla, L., Mazumder, R., et al. 2015, *ApJ*, 807, 71
 Pasachoff, J. M., Jacobson, W. A., & Sterling, A. C. 2009, *Sol. Phys.*, 260, 59
 Pesnell, W. D., Thompson, B. J., & Chamberlin, P. C. 2012, *Sol. Phys.*, 275, 3
 Priest, E. R., Heyvaerts, J. F., & Title, A. M. 2002, *ApJ*, 576, 533
 Qi, Y., Huang, Z., Xia, L., et al. 2019, *Sol. Phys.*, 294, 92
 Raouafi, N. E., Patsourakos, S., Pariat, E., et al. 2016, *Space Sci. Rev.*, 201, 1
 Raouafi, N. E., Petrie, G. J. D., Norton, A. A., Henney, C. J., & Solanki, S. K. 2008, *ApJ*, 682, L137
 Raouafi, N. E. & Stenborg, G. 2014, *ApJ*, 787, 118
 Rouppe van der Voort, L., De Pontieu, B., Pereira, T. M. D., Carlsson, M., & Hansteen, V. 2015, *ApJ*, 799, L3
 Rouppe van der Voort, L., Leenaarts, J., de Pontieu, B., Carlsson, M., & Vissers, G. 2009, *ApJ*, 705, 272
 Rouppe van der Voort, L. H. M., De Pontieu, B., Hansteen, V. H., Carlsson, M., & van Noort, M. 2007, *ApJ*, 660, L169
 Samanta, T., Tian, H., Yurchyshyn, V., et al. 2019, *Science*, 366, 890
 Schou, J., Scherrer, P. H., Bush, R. I., et al. 2012, *Sol. Phys.*, 275, 229
 Sekse, D. H., Rouppe van der Voort, L., & De Pontieu, B. 2012, *ApJ*, 752, 108
 Sekse, D. H., Rouppe van der Voort, L., & De Pontieu, B. 2013, *ApJ*, 764, 164
 Shen, Y., Liu, Y. D., Su, J., Qu, Z., & Tian, Z. 2017, *ApJ*, 851, 67
 Sterling, A. C. 2000, *Sol. Phys.*, 196, 79
 Sterling, A. C., Moore, R. L., Falconer, D. A., & Adams, M. 2015, *Nature*, 523, 437
 Terradas, J., Andries, J., Goossens, M., et al. 2008, *ApJ*, 687, L115
 Tian, H., DeLuca, E. E., Cranmer, S. R., et al. 2014, *Science*, 346, 1255711
 Tian, H., McIntosh, S. W., Habbal, S. R., & He, J. 2011, *ApJ*, 736, 130
 Tian, H., Tu, C., Marsch, E., He, J., & Kamio, S. 2010, *ApJ*, 709, L88
 Tsiropoula, G., Tziotziou, K., Kontogiannis, I., et al. 2012, *Space Sci. Rev.*, 169, 181
 Wang, H. 1998, *ApJ*, 509, 461
 Wang, H., Johannesson, A., Stage, M., Lee, C., & Zirin, H. 1998, *Sol. Phys.*, 178, 55
 Wang, Y. M. & Muglach, K. 2008, *Sol. Phys.*, 249, 17
 Wang, Y. M. & Sheeley, N. R., Jr. 1995, *ApJ*, 452, 457
 Wang, Y. M., Sheeley, N. R., Dere, K. P., et al. 1997, *ApJ*, 484, L75
 Wang, Y. M., Warren, H. P., & Muglach, K. 2016, *ApJ*, 818, 203
 Wei, H., Huang, Z., Hou, Z., et al. 2020, *MNRAS*, 498, L104
 Wilhelm, K., Abbo, L., Auchère, F., et al. 2011, *A&A Rev.*, 19, 35
 Xia, L. D., Marsch, E., & Curdt, W. 2003, *A&A*, 399, L5
 Xia, L. D., Marsch, E., & Wilhelm, K. 2004, *A&A*, 424, 1025
 Xiang, Y.-y., Liu, Z., & Jin, Z.-y. 2016, *New A*, 49, 8
 Yang, Y.-F., Qu, H.-X., Ji, K.-F., et al. 2015, *Research in Astronomy and Astrophysics*, 15, 569
 Zhelyazkov, I., Chandra, R., & Srivastava, A. K. 2016, *Ap&SS*, 361, 51

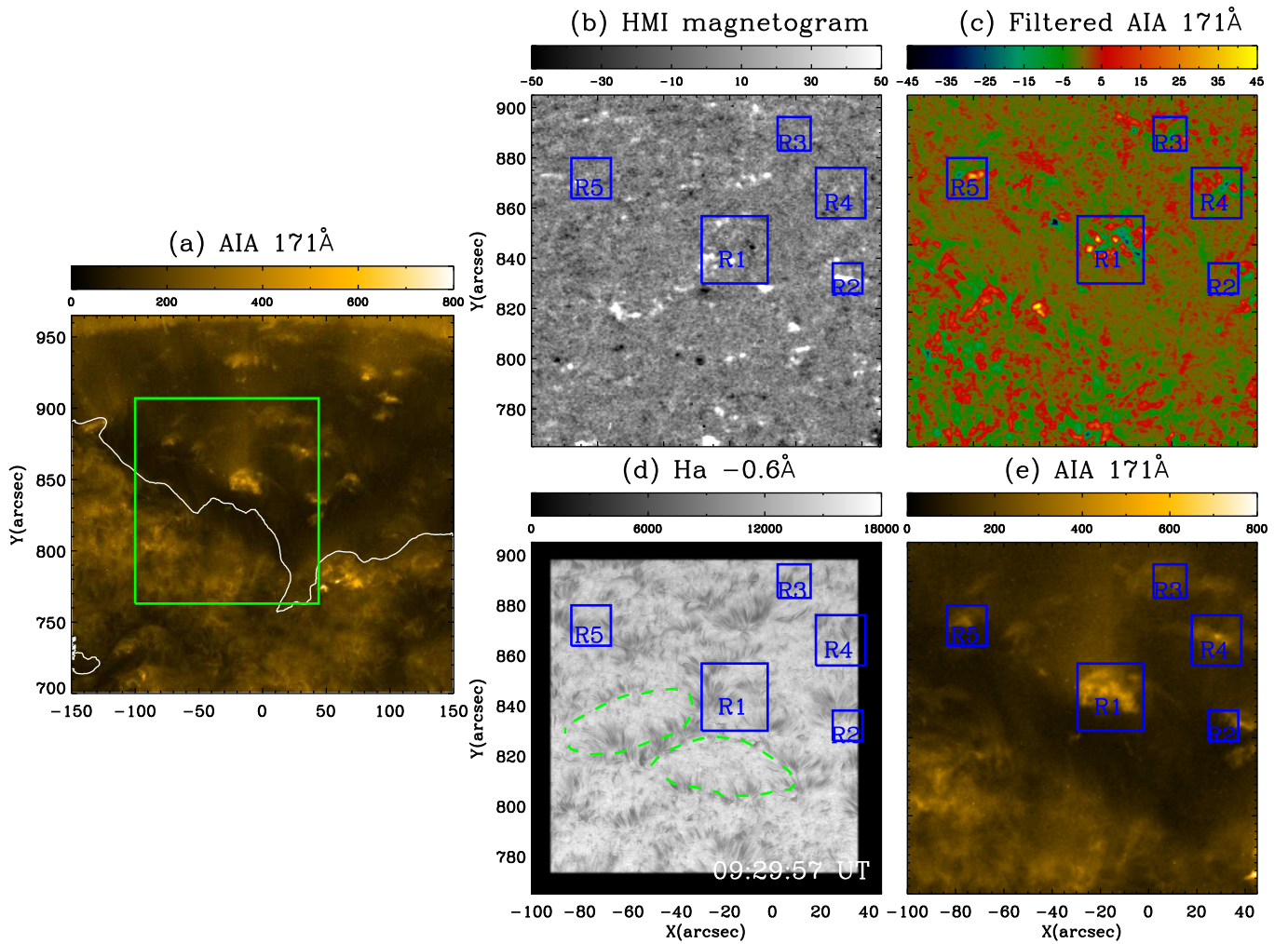


Fig. 1. Context images for regions studied in the present work taken on 2018 September 15. The AIA 171 Å image is giving an overview of the coronal structures in and around the studied regions (a). The contours (*white lines*) outline the boundaries of the coronal holes determined from the AIA 193 Å image. The region enclosed by the rectangle (green lines) is zoomed-in in panels (b–e). The region of interest seen with HMI magnetic features (b), AIA 171 Å filtered (10–30 minutes) image (c), NVST H α -0.6 Å image (d) and AIA 171 Å image (e) is shown. The rectangles (*blue lines*) in panels (b–e) mark the network regions where coronal plumes are clearly seen. The green dotted lines in panel (d) mark two full and clear network regions.

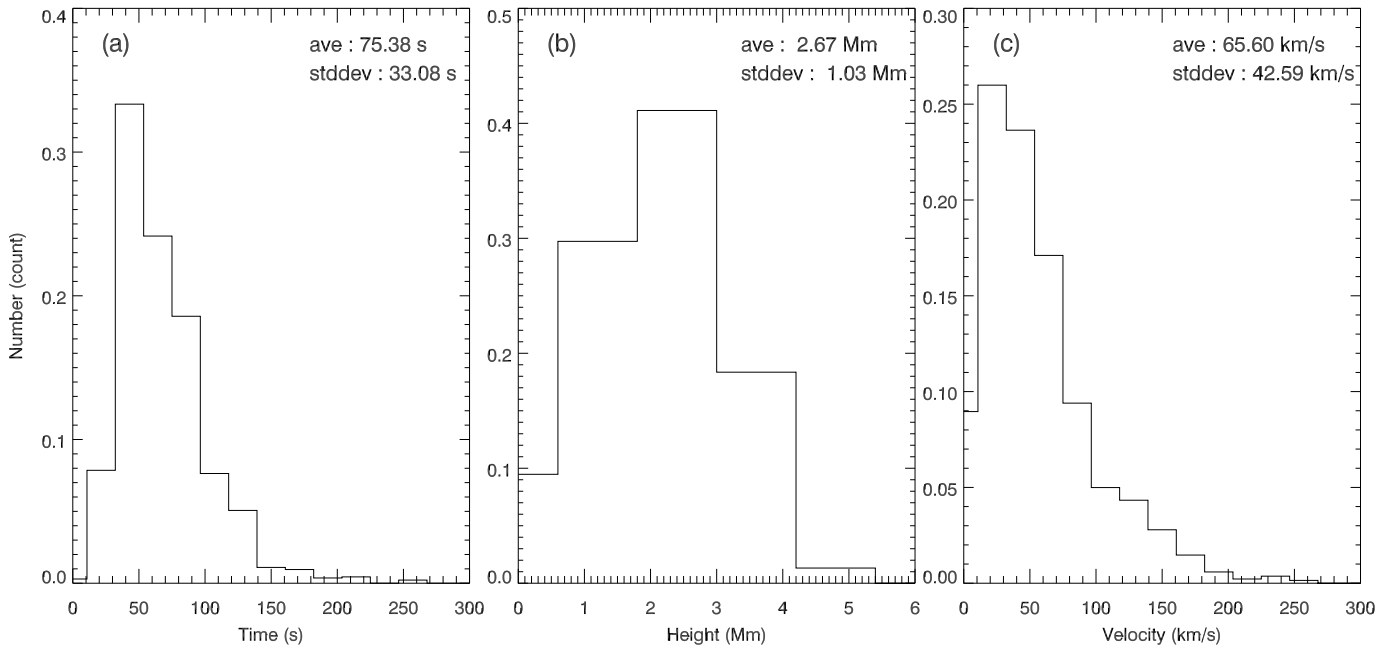


Fig. 2. The normalized distributions of the lifetimes (a), heights (b) and speeds (c) of the $H\alpha$ jets identified and tracked in the whole field-of-view. The values following to “ave” and “stddev” are the average values and standard deviations of the corresponding parameters, respectively.

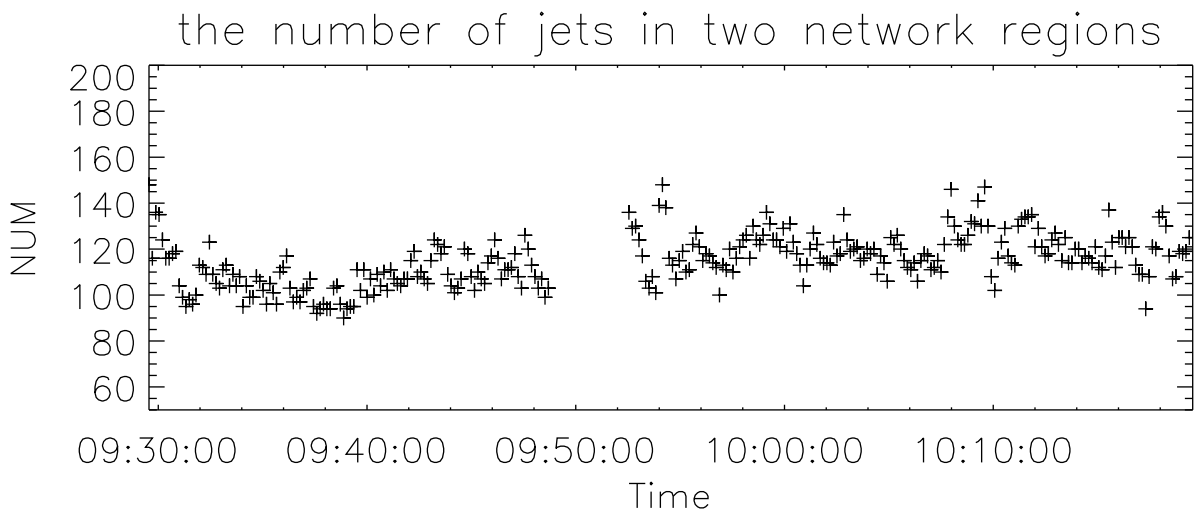


Fig. 3. Variation of the number of the $H\alpha$ jets identified in two network regions as marked in Figure 1d. The data around 09:50:00 have been removed due to bad observing conditions.

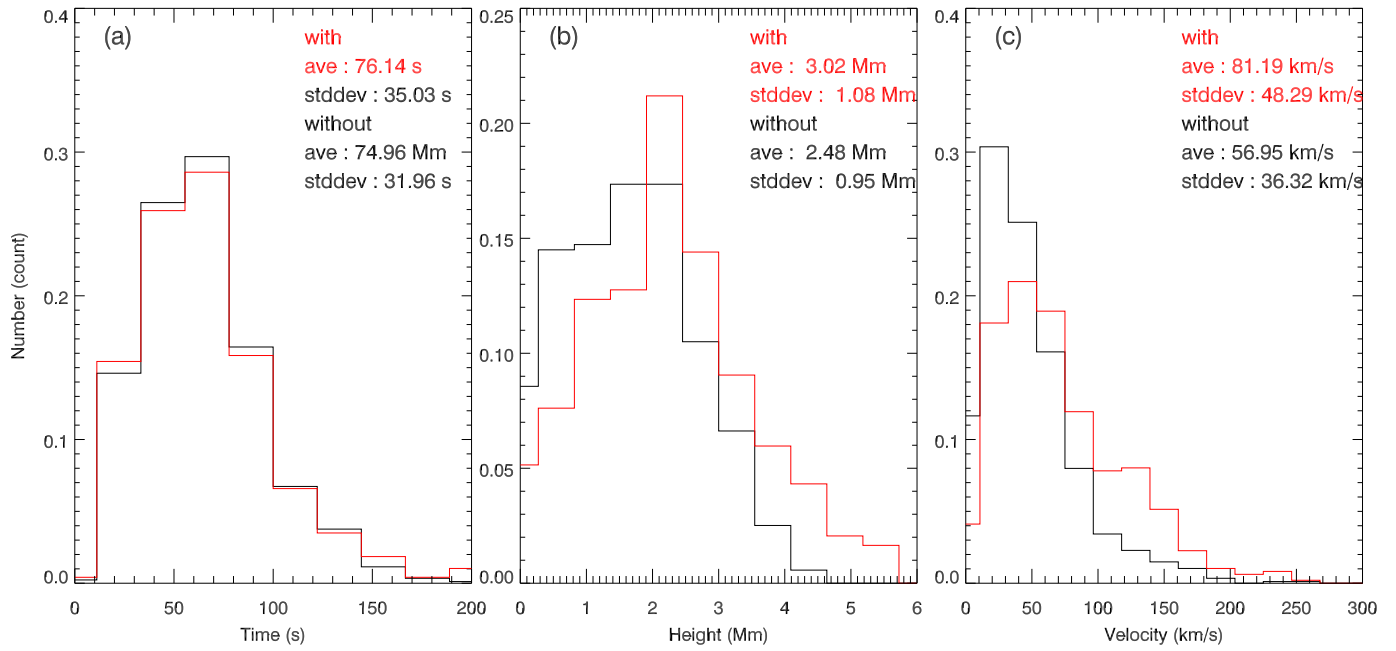


Fig. 4. The normalized distributions of the properties of (a) lifetimes, (b) heights and (c) velocities of the H α jets identified and tracked in the regions of R1 - R5 (*red lines*) and the rest regions (*black lines*). The values following to “ave” and “stddev” are the average values and standard deviations of the corresponding parameters, respectively.

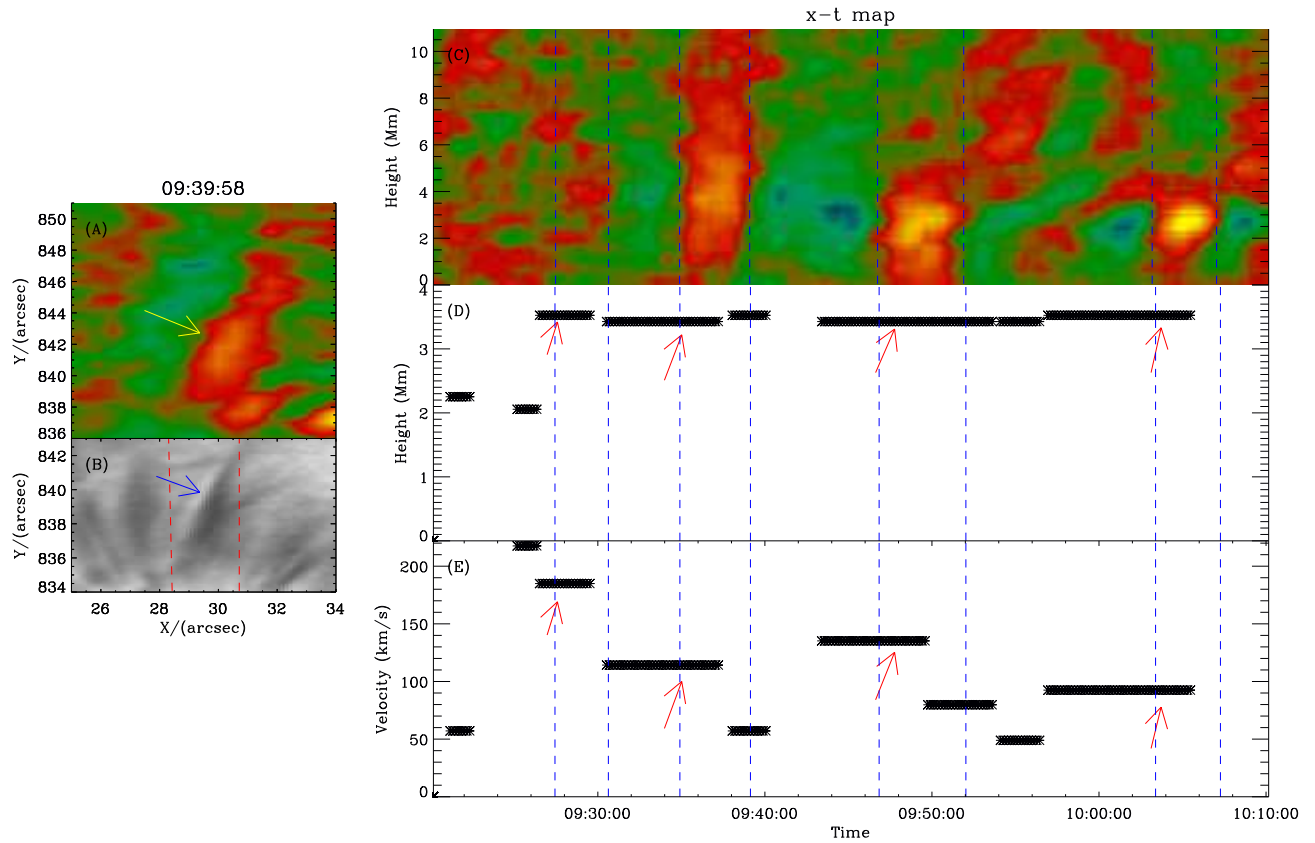


Fig. 5. A case analysis of the relationship between propagating disturbances (PDs) and $H\alpha$ jet. Snapshot showing the connection between $H\alpha$ jets in the NVST $H\alpha -0.6 \text{ \AA}$ (B) and PDs in the filtered AIA 171 \AA (A). The yellow arrow outlines the structures of PDs determined from panel (A), while the blue arrow represents the associated $H\alpha$ jets from panel (B). Time-slice images of the PD is shown in Panel (C). The blue lines mark the locations of PDs. The panel (D) & (E) show that the the maximum height and ascending velocity of the $H\alpha$ jets which exist in the footpoint of the given PD. Those denoted by the red arrows are the ones presented prior to the PD.

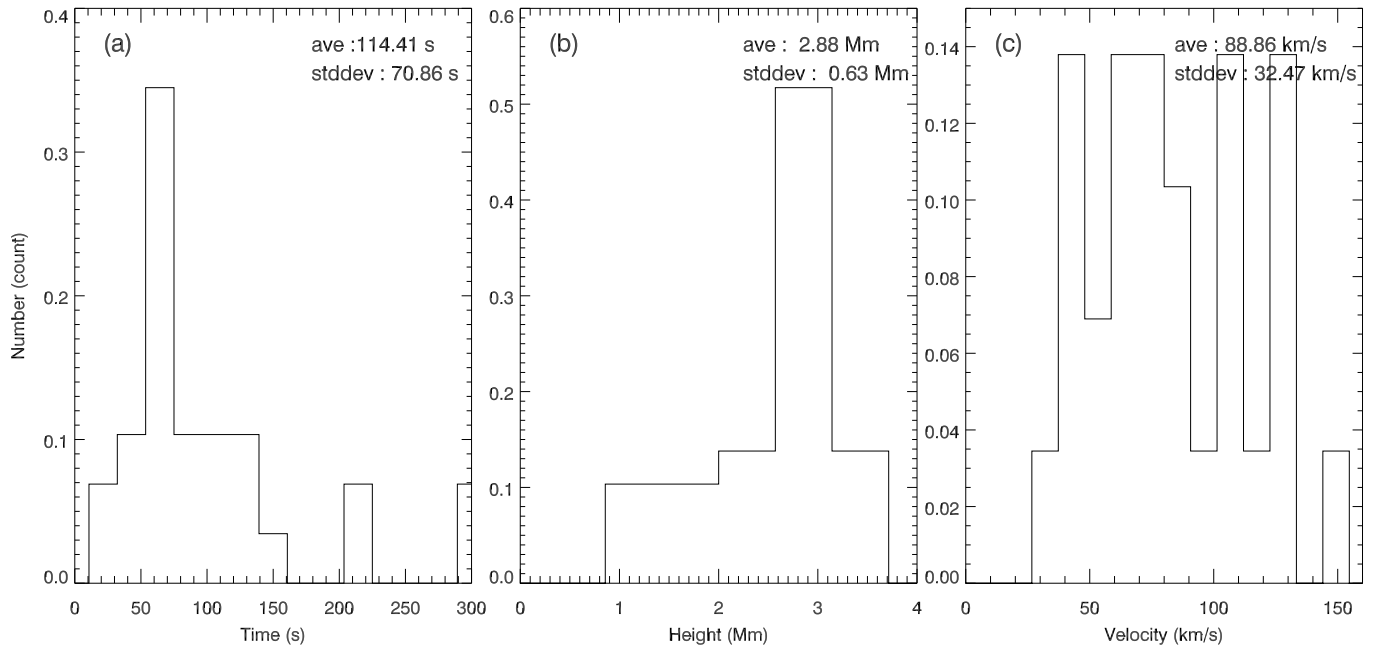


Fig. 6. The normalized distributions of the lifetimes (a), heights (b) and velocities (c) of the H α jets which have PDs response.

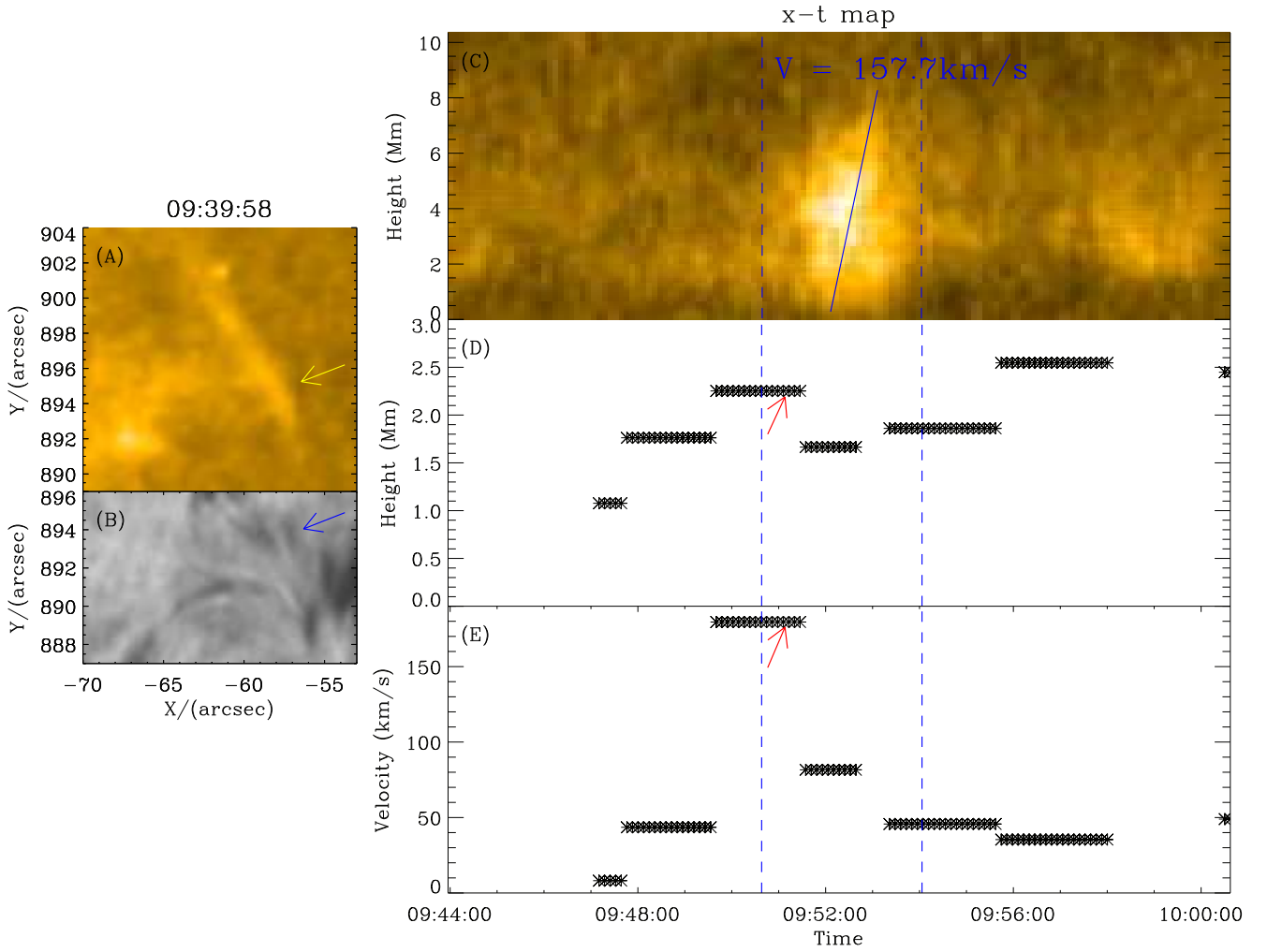


Fig. 7. A case analysis of the relationship between coronal jet and $H\alpha$ jet. Snapshot showing the connection between $H\alpha$ jets in the NVST $H\alpha - 0.6 \text{ \AA}$ (B) and coronal jet in the AIA 171 \AA (A). The yellow arrow outlines the structures of coronal jet determined from panel (A), while the blue arrow represents the $H\alpha$ jets from panel (B). Time-slice images of the coronal jet is shown in Panel (C), the velocity is 158 km s^{-1} . The panel (D) & (E) show that the the maximum height and ascending velocity of the $H\alpha$ jets which exist in the footpoint of the given coronal jet (seen those denoted by the red arrows). **The blue dashed lines indicate the location of the coronal jet.**